RESEARCH ARTICLE
doi: 10.2306/scienceasia1513-1874.2026.091

ScienceAsia 52 (5): 2026: ID 2026091: **1–9**

Mechanism of action of *Oxalis corniculata* L. extract in traditional Chinese medicine for the treatment of kidney stones

Fang Zhao†, Yu-Sheng Xu†, Jin-Feng Zhao, Kun-Mei Wang, Xiao-Ran Xiong, Feng Zhao*

Key Laboratory of Ethnic Medical Resources Research and Southeast Asian International Cooperation in Yunnan Province & School of Tea and Coffee & International Joint Laboratory of Digital Protection and Germplasm Innovation and Application of China-Laos Tea Tree Resources in Yunnan Province, Pu'er University, Yunnan 665000 China

*Corresponding author, e-mail: yu17608729717@126.com
† These authors contributed equally to this work.

Received 3 Nov 2025, Accepted 23 Sep 2026
Available online 12 Nov 2026

ABSTRACT: Renal calculi disease poses a significant challenge to both the health and quality of life of affected individuals. *Oxalis corniculata* L. has long been used in the treatment of this condition; however, mechanistic studies remain lacking. In this study, LC-MS/MS analysis of the aqueous extract of *O. corniculata* L. enabled the identification of 333 compounds. By integrating data from multiple compound databases and corroborating findings with the scientific literature, 53 of these compounds were confidently annotated as bioactive. Network pharmacological analysis indicated the potential of *O. corniculata* L. in treating renal calculi disease. This potential was experimentally validated in a rat model of calcium oxalate nephrolithiasis induced by concurrent administration of 2% ethylene glycol and 3% ammonium chloride. Treatment with *O. corniculata* L. significantly inhibited calcium oxalate stone formation. The therapeutic mechanisms may involve the antioxidative activity of *O. corniculata* L., which potentially reduces oxidative stress in renal cells, along with modulation of multiple signaling pathways such as AMPK, which enhances cellular energy metabolism; NF-kappa B, which modulates inflammation; HIF-1, which affects cellular responses to hypoxia; and PI3K-Akt, which plays a role in cell survival and proliferation. In summary, our study not only validates the efficacy of *O. corniculata* L. in treating renal calculi but also lays the foundation for subsequent clinical trials and in-depth investigation into its pharmacological properties.

KEYWORDS: *Oxalis corniculata* L., kidney stones, renal cells, medicinal compounds

INTRODUCTION

The formation of kidney stones is a common occurrence, affecting a significant portion of the global population. Prevalence rates are notably high, with 8.8% in the United States, 6.4% in China, and 3.5% in Korea [1–4], and continue to rise steadily [5]. Kidney stones not only have a high recurrence rate—approximately 50% within 5–10 years and up to 75% within 20 years [6, 7]—but also contribute to the development of obesity, diabetes, hypertension, chronic kidney disease, and other diseases [8].

The emergence of techniques such as endoscopic stone retrieval and extracorporeal shock wave lithotripsy (ESWL) has significantly advanced the treatment of renal calculi, albeit at considerable cost [7]. Given the high costs and potential complications associated with surgical treatments, there is a pressing need to explore non-surgical modalities to prevent the recurrence of urolithiasis.

Oxalis corniculata L., a traditional Chinese medicinal plant belonging to the Oxalidaceae family, is distributed across Asia, Europe, the Americas, and Africa, and is known for its various bioactive compounds [9, 10]. While research suggests that extracts of *O. corniculata* L. may possess anticancer [11, 12], antioxidant [13], antimicrobial [14, 15], antifungal [16], insecticidal [16], detoxifying [17–19], and anti-ulcer properties [20], there is a notable lack of research on its use in treating kidney stone disease.

Therefore, this study aims to elucidate the therapeutic efficacy and underlying mechanisms of *O. corniculata* L. in the treatment of kidney stone disease. Compound profiling of the aqueous extract of *O. corniculata* L. was conducted using LC-MS/MS, and subsequent network pharmacology analysis identified multiple bioactive compounds and their associated molecular targets implicated in kidney stone pathogenesis. A calcium oxalate kidney stone model was established in rats to investigate the therapeutic effects of *O. corniculata* L. Preliminary exploration of the molecular mechanisms was conducted using bioinformatics analysis. This study provides initial evidence of the efficacy of *O. corniculata* L. in treating kidney stone disease and explores its potential mechanisms of action.

MATERIALS AND METHODS

Plant materials

The specimen of *O. corniculata* L. was collected from tea plantations and vegetable gardens in the vicinity of Simao District, Pu'er City, Yunnan Province (101°00′ E, 22°45′ N). The plant was identified by sequencing the internal transcribed spacer (ITS) region of the ribosomal DNA using polymerase chain reaction (PCR).

The primers ITS2-F: ATGCGATACTTGGTGTGAAT and ITS2-R: GACGCTTCTCCAGACTACAAT were used for amplification. The collected *O. corniculata* L. was washed, dried at 50 °C, and ground into powder.

Extraction of active ingredients from *O. corniculata* L.

To extract active ingredients from *O. corniculata* L., a suitable amount of the plant powder was weighed and mixed with water at 10 and 8 times the weight of the plant powder for the first and second reflux extractions, respectively, using a reflux extraction apparatus (model DZTW, Bonsi Instrument Technology Co., Ltd., Beijing, China). The filtrates obtained from the two extractions were combined and concentrated under reduced pressure using a rotary evaporator (model RE-52, Shanghai Yarong Biochemical Instrument Factory, Shanghai, China) at 50 °C to remove the solvent. Lastly, the obtained extract was subjected to vacuum freeze-drying (freeze dryer, model FD-1A-50, Shanghai Jingxue Scientific Instrument Co., Ltd., Shanghai, China) to produce the aqueous extract of *O. corniculata* L.

Determination of active components in *O. corniculata* L.

The aqueous extract of *O. corniculata* L. was dissolved in 1% formic acid and ultrapure water, centrifuged to collect the supernatant, and filtered through a 0.22 μm membrane. Compound identification was performed using liquid chromatography-tandem mass spectrometry (LC-MS/MS) in both positive and negative ionization modes on a Q-Exactive mass spectrometer (Thermo Fisher Scientific, Waltham, MA, USA). The analytical column used was a Thermo Scientific Hypersil GOLD™ aQ (100 × 2.1 mm, Thermo Fisher Scientific). The LC-MS/MS conditions were set as follows: mobile phase A was 1% formic acid in water, mobile phase B was methanol, the flow rate was 0.2 ml/min, and the gradient elution was as follows: 0–1 min, 2% B; 1–23 min, linear increase to 98% B; 23–25 min, 98% B; 25–30 min, 2% B.

Mass spectrometry analysis

Compound mass spectral data from *O. corniculata* L. aqueous extract were collected via first-level mass spectrometry (MS1) and second-level mass spectrometry (MS2). The acquired spectral data were processed using Xcalibur and Compound Discoverer software to ascertain the identities of the compounds. Compound classes and functionalities were determined by referencing metabolite databases such as PubChem (https://pubchem.ncbi.nlm.nih.gov, accessed on 25 December 2023), FunMeta v1 (http://funmeta.oebiotech.cn/search, accessed on 25 December 2023), the ChemSrc website (https://www.chemsrc.com, accessed on 25 December 2023), and relevant literature sources.

Animal feeding and construction of a calcium oxalate kidney stone model

Male Sprague-Dawley (SD) rats (200 ± 20 g) were procured from the Department of Experimental Animals, Kunming Medical University, Yunnan, China (Biological Production License No.: SCXK (Dian), K2015-0002). Animals were randomly allocated into five groups: control, model, positive control, medium-dose (0.6 g/kg), and high-dose (1.12 g/kg) groups, with 5 rats per group. During the construction of the calcium oxalate renal stone animal model, the control group received normal feed (15 g/rat/day). The model, positive control, medium-dose, and high-dose groups were fed feed containing 2% ethylene glycol and 3% ammonium chloride (15 g/rat/day) for 12 days. Starting on Day 13, the control and model groups received daily oral gavage of sterile distilled water (ddH_2O; 1 ml/100 g body weight), whereas the positive control group, medium-dose group, and high-dose group received equivalent volumes—calculated based on daily body weight measurements—of sodium potassium hydrogen citrate granule solution, *O. corniculata* L. aqueous extract solution, respectively, for 12 consecutive days. The feed provided during the treatment period remained unchanged. Throughout the entire experimental period, water consumption was controlled at 30 ml/rat/day.

MDA content determination

Serum samples: Blood was collected from the abdominal aorta of rats after 24-h urine collection, and serum was separated by centrifugation at 3,000 rpm for 10 min. The serum was diluted, and Ca^{2+} and Mg^{2+} contents were determined using atomic absorption spectrophotometry (Beijing Persee General Instrument Co., Ltd., Beijing, China).

Kidney tissue samples: A fixed amount of kidney tissue was taken, digested with nitric acid at high temperature, cooled, diluted to volume, and then centrifuged to obtain the supernatant. The Ca^{2+} content in the supernatant was measured using the same atomic absorption method.

The samples were homogenized in ice-cold trichloroacetic acid (TCA), and the homogenates were subsequently centrifuged. The supernatant was collected and mixed with thiobarbituric acid (TBA) chromogenic reagent. The mixture was heated in a boiling water bath, followed by cooling and a second centrifugation. The absorbance of the final supernatant was determined at 532 nm (A_{532}) and 600 nm (A_{600}). The MDA content was calculated using the following formula: MDA content (nmol/ml) $= (A_{532} - A_{600})/(\varepsilon \times L) \times$ dilution factor, where ε represents the molar extinction coefficient (155 $mM^{-1}cm^{-1}$), and L refers to the optical path length.

Determination of Ca^{2+} and Mg^{2+} levels in serum and renal tissue

Determination of urinary protein levels in each group of rats

A series of albumin standard solutions at different concentrations were prepared, and a corresponding concentration-absorbance standard curve was established. The supernatant was collected from centrifuged rat urine samples for subsequent analysis. Equal volumes of urine samples and albumin standard solutions were separately mixed with sulfosalicylic acid-sodium sulfate turbidimetric reagent, and all mixtures were incubated at room temperature to complete the reaction. The spectrophotometer was calibrated to 590 nm and zeroed with blank reagent. The absorbance values of standard tubes and sample tubes were measured in order. Finally, the urinary protein content of all rat samples was calculated according to the fitted standard curve.

Preparation and observation of renal tissue histological sections

H&E staining: Paraffin-embedded kidney tissue sections were dewaxed and rehydrated. Tissue nuclei were stained with hematoxylin, and then the cytoplasm as well as interstitial components were stained with eosin. Subsequently, differentiation, dehydration, clearing, and mounting were performed sequentially. The intact renal tissue structure, cellular morphology, and pathological lesions, including inflammatory infiltration and tissue injury, were clearly observed under a microscope.

Von Kossa staining: All sections were dewaxed and rehydrated before being incubated in silver nitrate solution under dark conditions. A specific color reaction was triggered between calcium salts and silver ions under light irradiation. Afterwards, the sections were decolorized with sodium thiosulfate solution and fully rinsed with distilled water. Routine dehydration, clearing, and mounting procedures were conducted in sequence. This staining approach was used to specifically detect calcium salt deposition in renal tissues, and positive calcium deposits appeared as brown-black regions.

RESULTS

O. corniculata L. is rich in bioactive compounds and medicinal constituents.

To determine the composition of compounds in *O. corniculata* L., we utilized the LC-MS/MS technique following the procedure outlined in Fig. 1A to analyze the constituents of the aqueous extract of *O. corniculata* L. Specifically, using positive ion mode, we identified 120 and 209 compounds in the *O. corniculata* L. aqueous extract dissolved in 1% formic acid and ultrapure water, respectively (Table S1, Table S2). Using negative ion mode, we identified 91 and 132 compounds in the *O. corniculata* L. aqueous extract dissolved in 1% formic acid and ultrapure water, respectively (Table S3, Table S4). After combining and deduplicating the identified compounds, we obtained 333 compounds (Table S5, Fig. 1B). By integrating data from the PubChem, FunMeta v1, and ChemSpider databases—along with previously published literature on these compounds—we identified 53 pharmacologically active compounds (Table S6). Based on the classification of compound types, these 53 active compounds could be sorted into 28 categories, with the flavonoid class being the most abundant, followed by benzene and substituted derivatives (Fig. 1C). These findings suggest the significant medicinal value of *O. corniculata* L.

O. corniculata L. possesses multiple potential targets for the treatment of kidney stones

To evaluate the therapeutic potential of *O. corniculata* L. in kidney stone disease, we retrieved 324 putative drug targets of its bioactive compounds from the Traditional Chinese Medicine Systems Pharmacology (TCMSP) database. We screened 643 disease targets related to kidney stones from databases such as DrugBank, OMIM, PharmGKB, and GeneCards. By intersecting these disease targets with the potential targets of active ingredients from *O. corniculata* L., we identified 60 potential targets related to kidney stone disease (Fig. 2A). Furthermore, we observed that the active ingredients in *O. corniculata* L. were associated with multiple targets related to kidney stone disease, with quercetin and resveratrol each having over 35 potential targets (Fig. 2B). These findings suggest that *O. corniculata* L. may hold promise for the treatment of kidney stone disease.

O. corniculata L. possesses therapeutic effects in the treatment of nephrolithiasis

To evaluate the therapeutic efficacy of *O. corniculata* L. against kidney stone disease, a rat model of calcium oxalate nephrolithiasis was established by administering a diet containing 2% ethylene glycol and 3% ammonium chloride to the model group for 12 consecutive days, as shown in Fig. 3A. Starting from day 13, drug treatment was administered for 12 days while the same feed was maintained, followed by biochemical parameter measurements in urine, serum, and kidney on day 25. Post-modeling, the model rats exhibited hematuria and a significant reduction in body weight compared with the control group, confirming successful establishment of the animal model for subsequent validation experiments (Fig. 3B,C). Following drug treatment, renal indices, urinary protein concentration, serum calcium and magnesium levels, and renal cortical calcium content were measured in all rat groups. Results showed a significant increase in renal indices and urinary protein content in the model group compared with the control group. Both renal

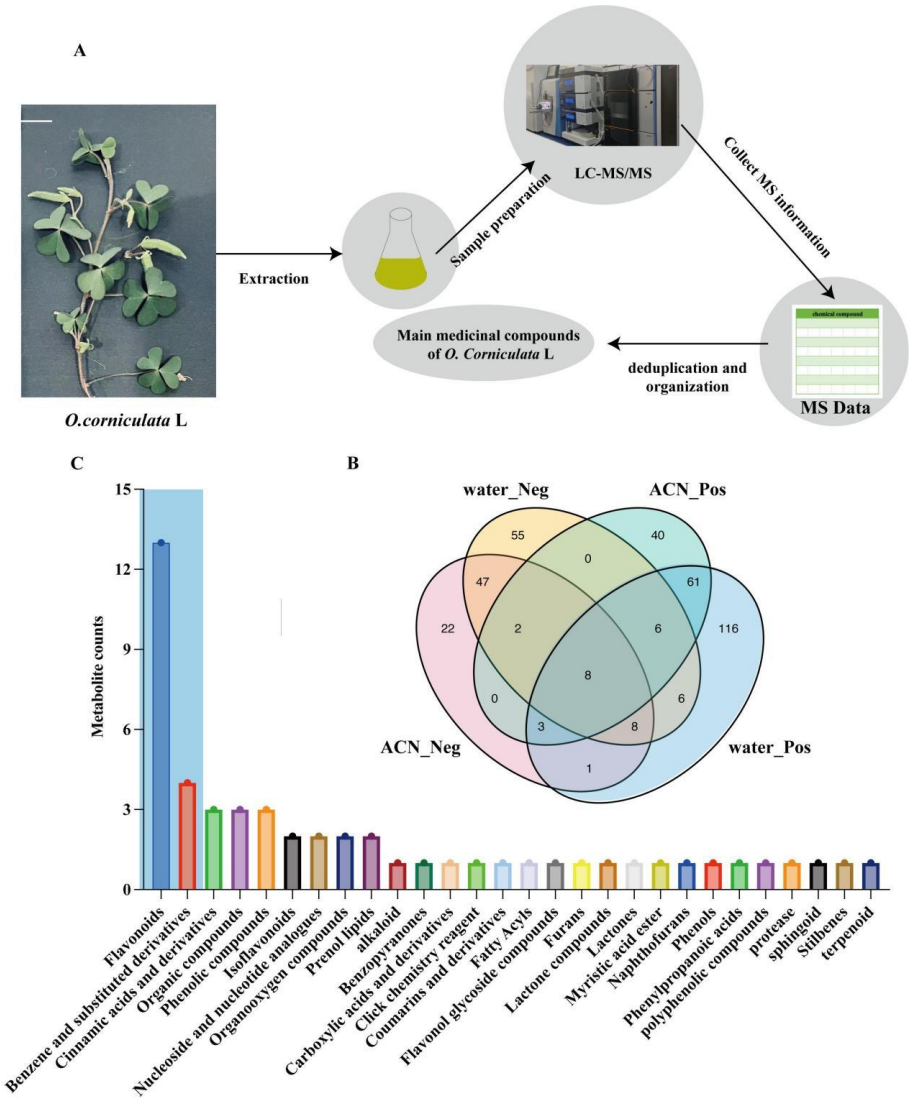

Fig. 1 Determination of chemical constituents and identification of active pharmaceutical ingredients in *O. corniculata* L. (A) Schematic diagram illustrating the process of compound determination in *O. corniculata* L. Bar = 10 mm. (B) Venn diagram showing compound numbers detected under four LC-MS/MS detection conditions (water_Neg, water_Pos, ACN_Neg, ACN_Pos). (C) Analysis of the compound composition of *O. corniculata* L. aqueous extract.

index and urinary protein level slightly decreased after drug treatment (Fig. 3D,E). Furthermore, an upward trend in Ca^{2+} content in kidney tissue and serum was observed in the model group compared with the control group, but the differences were not significant (Fig. 3F,G). Additionally, a decreasing trend in serum Mg^{2+} content after drug treatment was observed, albeit with no significant differences compared with the control and model groups (Fig. 3H).

O. corniculata L. has been demonstrated to possess potent antioxidant activity [21], suggesting that it may achieve therapeutic effects by scavenging excess free radicals in the body, reducing lipid peroxidation. To test this hypothesis, the content of malondialdehyde (MDA), a well-established biomarker of lipid peroxidation, was measured in the kidneys of each experimental group. The results showed that compared with the control group, the MDA content in the model group increased slightly, but the difference was not significant. Upon administration of different drug treatments, the MDA content decreased, particularly significantly in the dose group of *O. corniculata* L. aqueous extract (Fig. 4).

H&E staining and von Kossa staining results showed that in the blank control group, the boundary between the renal cortex and medulla was clear, the renal tubules were tightly arranged, the renal tubular epithelial cells were uniformly stained and normal in

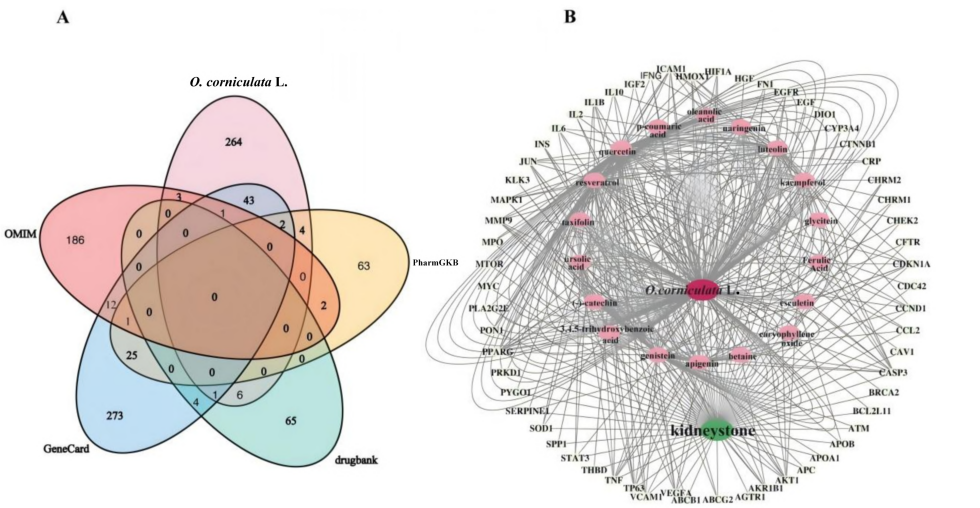

Fig. 2 Identification of the targets of action of *O. corniculata* L. (A) Analysis of kidney stone targets shared between *O. corniculata* L. and the DrugBank, OMIM, PharmGKB, and GeneCards databases. (B) Network pharmacology analysis of the medicinal components of *O. corniculata* L.

shape, the glomerular capillary tufts were distinct, and no calcium oxalate crystals were observed (Fig. 5A,B). In the stone model group, extensive tubular dilation and thinning of tubular walls (black arrows) were observed in the renal cortex and medulla, with a small amount of connective tissue hyperplasia in the local tubulointerstitium of the cortex (blue arrows), accompanied by inflammatory cell infiltration (red arrows). Calcium oxalate crystals were visible on von Kossa staining (yellow arrows) (Fig. 5C,D). In the kidneys of rats in the positive drug group, the corticomedullary boundary was clear. There was only mild tubular dilation with thinning of tubular walls (black arrows), a small amount of inflammatory cell infiltration around blood vessels (red arrows), occasional cystic dilation of renal tubules in the medulla, and a small number of inflammatory cells visible within the tubular lumens (yellow arrows) (Fig. 5E,F). In the kidneys of rats in the medium-dose group receiving the aqueous extract of *O. corniculata* L., there was more pronounced tubular dilation in the cortical region with thinning of tubular walls (black arrows), and a small number of renal tubular epithelial cells showed mild swelling with vacuolated cytoplasm (red arrows) (Fig. 5G,H). In the kidneys of rats in the high-dose group receiving the aqueous extract of *O. corniculata* L., there was mild tubular dilation with thinning of tubular walls (black arrows), and a larger number of renal tubular epithelial cells showed swelling with vacuolated cytoplasm (red arrows) (Fig. 5I,J).

O. corniculata L. has the potential to modulate multiple signaling pathways

In order to further explore the mechanisms by which *O. corniculata* L. treats kidney stone disease, we conducted GO functional enrichment and KEGG pathway analyses of the potential kidney stone disease targets of active components in *O. corniculata* L. The analysis results indicate that these target genes are primarily enriched in functions related to signal transduction, enzyme activity regulation, protein transport, cytokines, intercellular communication, and transcription factors (Fig. S1). They operate within key signaling pathways, including AGE-RAGE, fluid shear stress and atherosclerosis, HIF-1, TNF, JAK-STAT, PI3K-Akt, IL-17, NF-kappa B, TGF-β, MAPK, Wnt, and AMPK. Among these pathways, AMPK [22], NF-kappa B [23], HIF-1 [24], and PI3K-Akt [25] have been demonstrated to be associated with kidney stone disease (Fig. S2). This suggests that the pharmacological components in *O. corniculata* L. may target certain factors within these signaling pathways to regulate the progression of kidney stone disease. The specific mechanisms require further experimental exploration. At the same time, a protein-protein interaction network analysis was performed on these disease targets, revealing strong interaction relationships between STAT3, AKT1, TNF, IL6, and other target proteins (Fig. 6).

DISCUSSION

In traditional Chinese medicine, *O. corniculata* L. is commonly used for the treatment of nephrolithiasis. Despite its traditional use, the scientific validation of *O. corniculata* L. is crucial to integrate this herbal treatment into mainstream medical practices. However, there is a lack of research on the efficacy validation and mechanisms of *O. corniculata* L. in treating nephrolithiasis, necessitating further investigation and supplementation. Our study reveals that *O. corniculata* L. contains various drug components associated with

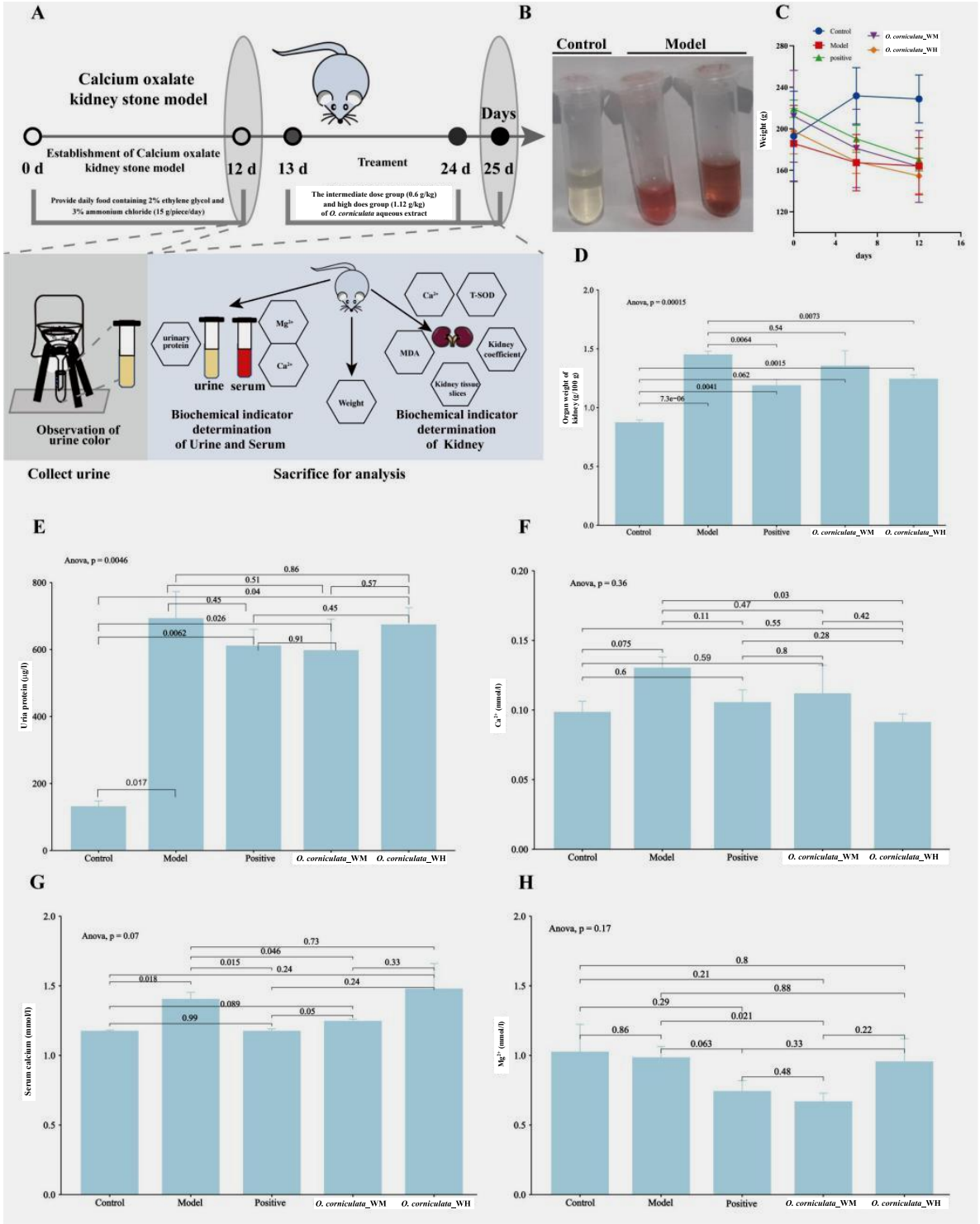

Fig. 3 Validation of the efficacy of *O. corniculata* L. in treating nephrolithiasis. (A) Schematic representation of the efficacy validation of *O. corniculata* L. (B) Observation of urine color. (C) During the modeling phase, alterations in body mass observed. (D) Measurement of the renal coefficient. (E) Determination of urinary protein levels. (F, G) Measurement of Ca^{2+} content in renal tissue and serum. (H) Measurement of Mg^{2+} content in renal tissue and serum. (D) to (H) Performed in each group of rats. Error bars represent the standard deviation (SD).

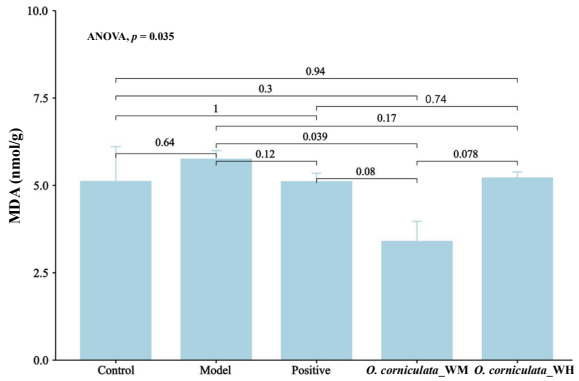

Fig. 4 Determination of MDA levels in each group of rats. The numbers in the figure represent p-values. A p-value $\leqslant 0.05$ indicates a statistically significant difference.

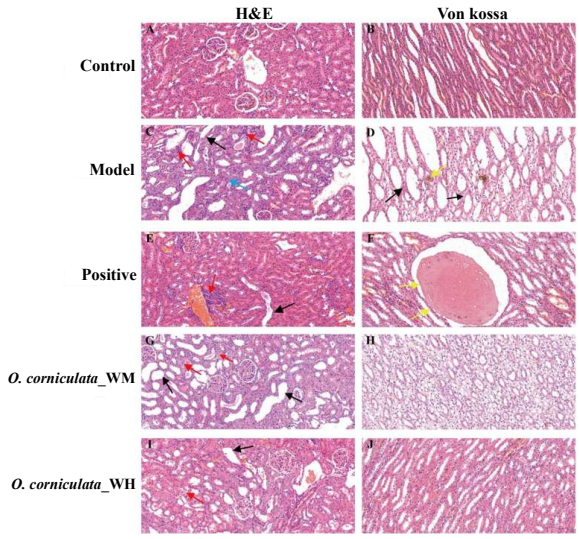

Fig. 5 Pathological section analysis of renal tissue. Kidney tissue sections from (A, B) rats in the control group; (C, D) rats in the stone model group; (E, F) rats treated with potassium citrate granules as the positive control; (G, H) rats treated with a medium dose of aqueous extract from the *O. corniculata* L.; (I, J) rats treated with a high dose of aqueous extract from *O. corniculata* L.

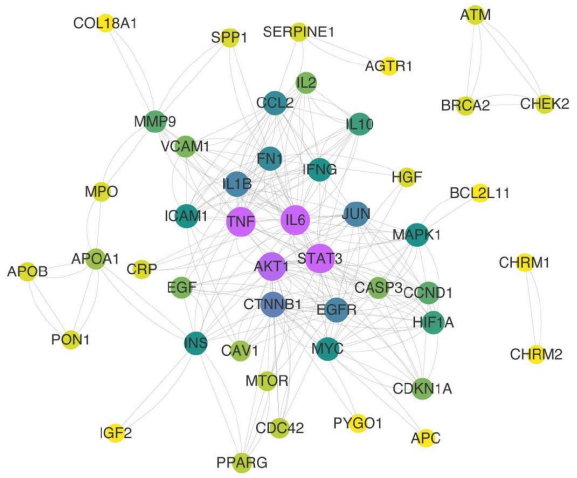

Fig. 6 Analysis of the protein-protein interaction network of target proteins.

therapeutic targets for nephrolithiasis. In our rodent models, administration of *O. corniculata* L. significantly reduced the size and number of calcium oxalate stones, demonstrating its therapeutic potential [26]. Within plants, it facilitates physiological processes such as seed germination, pollen growth, and antioxidation, crucial for plant responses to both stress and non-stress environments [27]. Research indicates quercetin's potential as an antiviral agent, as it inhibits the initial stages of viral infection by interacting with key viral replicative enzymes and reducing inflammation caused by infection [26]. In preclinical models of rheumatoid arthritis, gouty arthritis, and osteoarthritis, quercetin exhibits significant joint protective effects [28]. Additionally, its antioxidant properties, ability to promote apoptosis, and efficacy in preventing or alleviating cancer have been documented [29]. Furthermore, quercetin has been identified as a therapeutic agent for reducing the formation of oxalate stones, particularly in patients with recurrent oxaluria-associated lithiasis [30, 31].

We quantified compounds in *O. corniculata* L. using LC-MS/MS and successfully identified quercetin and resveratrol as active constituents. Furthermore, network pharmacology analysis identified over 35 potential therapeutic targets associated with nephrolithiasis that are modulated by these two active ingredients. These findings suggest that quercetin and resveratrol may contribute to the therapeutic efficacy of *O. corniculata* L. against nephrolithiasis.

Research has indicated that Mg^{2+} can form complexes with oxalate in the body, thereby reducing the aggregation and growth of calcium oxalate crystals, which helps reduce stone formation [32]. In our experiment, we found that the serum Mg^{2+} content was similar between the control and model groups. However, in the medium-dose *O. corniculata* L. aqueous extract group and the positive control group, the serum Mg^{2+} content was significantly decreased compared with the control and model groups. This suggests that *O. corniculata* L. aqueous extract may facilitate the complexation of Mg^{2+} with oxalate. Nevertheless, further investigation is needed to elucidate this potential mechanism.

Free radicals exert a pathogenic role in kidney stone formation by mediating lipid peroxidation-induced cellular membrane damage, facilitating the deposition and retention of calcium oxalate crystals, and thereby promoting lithogenesis [33]. However, our research indicates that in rats induced to form

stones by 2% ethylene glycol and 3% ammonium chloride, there was a significant decrease in MDA levels following treatment with *O. corniculata*_WM. This finding suggests that the antioxidant components in *O. corniculata* L. play a crucial role in the treatment of renal stone disease.

GO enrichment and KEGG pathway analyses of the 60 kidney stone disease targets corresponding to the active components of *O. corniculata* L. revealed that these disease targets are primarily associated with AMPK, NF-kappa B, HIF-1, and PI3K-Akt pathways, without specific elucidation of the underlying mechanisms. Research indicates that oxalate induces renal tubular epithelial cell calcification and participates in kidney stone formation through activation of the JAK2/STAT3 signaling pathway [34]. TNFR signaling contributes to inflammation and renal calcium deposition in oxalate nephropathy [35]. This suggests that STAT3 and TNF may serve as critical therapeutic targets for kidney stone diseases.

CONCLUSION

Our study has to some extent confirmed the efficacy of *O. corniculata* L. in treating kidney stones and has preliminarily explored the potential mechanisms of *O. corniculata* L. in treating this disease. This has contributed to the knowledge in this research field and laid the foundation for further in-depth studies.

Appendix A. Supplementary data

Supplementary data associated with this article can be found at https://dx.doi.org/10.2306/scienceasia1513-1874.2026.091. Tables S1–S4 are available from the corresponding author upon reasonable request.

Acknowledgements: This work was supported by grants from the Chinese National Natural Science Foundation (82260851, 81860696, and 31560596) and the "Yunnan Scholar" Program (2019HB058).

REFERENCES

1. Scales CD Jr, Smith AC, Hanley JM, Saigal CS (2012) Urologic diseases in America project. Prevalence of kidney stones in the United States. *Eur Urol* **62**, 160–165.
2. Zeng G, Mai Z, Xia S, Wang Z, Zhang K, Wang L (2017) Prevalence of kidney stones in China, an ultrasonography based cross-sectional study. *BJU Int* **120**, 109–116.
3. Tsai CH, Chen YC, Chen LD, Pan TC, Ho CY, Lai MT, Tsai FJ, Chen WC, et al (2008) A traditional Chinese herbal antilithic formula, Wulingsan, effectively prevents the renal deposition of calcium oxalate crystal in ethylene glycol-fed rats. *Urol Res* **36**, 17–24.
4. Yan X, Xia Y, Li B, Ye Z, Li L, Yuan T, Song B, Yu W, et al (2024) The SOX4/EZH2/SLC7A11 signaling axis mediates ferroptosis in calcium oxalate crystal deposition-induced kidney injury. *J Transl Med* **22**, 9.
5. Thongprayoon C, Krambeck AE, Rule AD (2020) Determining the true burden of kidney stone disease. *Nat Rev Nephrol* **16**, 736–746.
6. Moe OW (2006) Kidney stones: Pathophysiology and medical management. *Lancet* **367**, 333–344.
7. Zhou J, Jin J, Li X, Zhao Z, Zhang L, Wang Q, Li J, Zhang Q, et al (2018) Total flavonoids of *Desmodium styracifolium* attenuates the formation of hydroxy-L-proline-induced calcium oxalate urolithiasis in rats. *Urolithiasis* **46**, 231–241.
8. Khan SR, Pearle MS, Robertson WG, Gambaro G, Canales BK, Doizi S, Traxer O, Tiselius HG, et al (2016) Kidney stones. *Nat Rev Dis Primers* **2**, 16008.
9. Abu-Elfotuh K, Hamdan AME, Mohamed SA, Bakr RO, Ahmed AH, Atwa AM, Hamdan AM, Alanzai AG, et al (2024) The potential anti-Alzheimer's activity of *Oxalis corniculata* Linn. methanolic extract in experimental rats: Role of APOE4/LRP1, TLR4/NF-κβ/NLRP3, wnt 3/β-catenin/GSK-3β, autophagy and apoptotic cues. *J Ethnopharmacol* **324**, 117731.
10. Sarfraz I, Rasul A, Hussain G, Shah MA, Nageen B, Jabeen F, Selamoğlu Z, Uçak İ, et al (2022) A review on phyto-pharmacology of *Oxalis corniculata*. *Comb Chem High Throughput Screen* **25**, 1181–1186.
11. Gholipour AR, Jafari L, Ramezanpour M, Evazalipour M, Chavoshi M, Yousefbeyk F, Kargar Moghaddam SJ, Yekta Kooshali MH, et al (2022) Apoptosis effects of *Oxalis corniculata* L. extract on human MCF-7. *Breast Cancer Cell Line Galen Med J* **11**, e2484.
12. Salahuddin H, Mansoor Q, Batool R, Farooqi AA, Mahmood T, Ismail M, et al (2016) Anticancer activity of *Cynodon dactylon* and *Oxalis corniculata* on Hep2 cell line. *Cell Mol Biol* **62**, 60–63.
13. Gao T, Hu W, Zhang Z, Tang Z, Chen Y, Zhang Z, Yuan S, Chen T, et al (2022) An acidic polysaccharide from *Oxalis corniculata* L. and the preliminary study on its antioxidant activity. *J Food Biochem* **46**, e14235.
14. Golbarg H, Mehdipour Moghaddam MJ (2021) Antibacterial potency of medicinal plants including *Artemisia annua* and *Oxalis corniculata* against multi-drug resistance *E. coil*. *Biomed Res Int*, 9981915.
15. Mukherjee S, Koley H, Barman S, Mitra S, Datta S, Ghosh S, Paul D, Dhar P, et al (2013) *Oxalis corniculata* (Oxalidaceae) leaf extract exerts *in vitro* antimicrobial and *in vivo* anticolonizing activities against *Shigella dysenteriae* 1 (NT4907) and *Shigella flexneri* 2a (2457T) in induced diarrhea in suckling mice. *J Med Food* **16**, 801–809.
16. Rehman A, Rehman A, Ahmad I (2015) Antibacterial, antifungal, and insecticidal potentials of *Oxalis corniculata* and its isolated compounds. *Int J Anal Chem*, 842468.
17. Ahmad B, Khan MR, Shah NA (2015) Amelioration of carbon tetrachloride-induced pulmonary toxicity with *Oxalis corniculata*. *Toxicol Ind Health* **31**, 1243–1251.
18. Sreejith G, Jayasree M, Latha PG, Suja SR, Shyamal S, Shine VJ, Anuja GI, Sini S, et al (2014) Hepatoprotective activity of *Oxalis corniculata* L. ethanolic extract against paracetamol induced hepatotoxicity in Wistar rats and its *in vitro* antioxidant effects. *Indian J Exp Biol* **52**, 147–152.
19. Khan MR, Zehra H (2013) Amelioration of CCl(4)-induced nephrotoxicity by *Oxalis corniculata* in rat. *Exp Toxicol Pathol* **65**, 327–334.
20. Sakat SS, Tupe P, Juvekar A (2012) Gastroprotective efect of *Oxalis corniculata* (whole plant) on experimentally induced gastric ulceration in Wistar rats. *Indian J Pharm Sci* **74**, 48–53.
21. Ahmed D, Zara S, Baig H (2012) *In vitro* analysis of antioxidant activities of *Oxalis corniculata* Linn. fractions

in various solvents. *Afr J Tradit Complement Altern Med* **10**, 158–165.
22. Tian H, Liang Q, Shi Z, Zhao H (2023) Hyperoside ameliorates renal tubular oxidative damage and calcium oxalate deposition in rats through AMPK/Nrf2 signaling axis. *J Renin Angiotensin Aldosterone Syst*, 544554.
23. Song Q, Song C, Chen X, Xiong Y, Li L, Liao W, Xue L, Yang S (2023) FKBP5 deficiency attenuates calcium oxalate kidney stone formation by suppressing cell-crystal adhesion, apoptosis and macrophage M1 polarization via inhibition of NF-κB signaling. *Cell Mol Life Sci* **80**, 301.
24. Peng Y, Fang Z, Liu M, Wang Z, Li L, Ming S, Lu C, Dong H, et al (2021) Testosterone induces renal tubular epithelial cell death through the HIF-1αBNIP3 pathway. *J Transl Med* **19**, 146.
25. Yuan H, Zhang J, Yin X, Liu T, Yue X, Li C, Wang Y, Li D, et al (2021) The protective role of corilagin on renal calcium oxalate crystal-induced oxidative stress, inflammatory response, and apoptosis via PPAR-γ and PI3K/Akt pathway in rats. *Biotechnol Appl Biochem* **68**, 1323–1331.
26. Di Petrillo A, Orrù G, Fais A, Fantini MC (2022) Quercetin and its derivates as antiviral potentials: A comprehensive review. *Phytother Res* **36**, 266–278.
27. Singh P, Arif Y, Bajguz A, Hayat S (2021) The role of quercetin in plants. *Plant Physiol Biochem* **166**, 10–19.
28. Goyal A, Agrawal N (2022) Quercetin: A potential candidate for the treatment of arthritis. *Curr Mol Med* **22**, 325–335.
29. Ozsoy Gokbilen S, Becer E, Vatansever HS (2022) Senescence-mediated anticancer effects of quercetin. *Nutr Res* **104**, 82–90.
30. Guzel A, Yunusoglu S, Calapoglu M, Candan IA, Onaran I, Oncu M, Ergun O, Oksay T, et al (2021) Protective effects of quercetin on oxidative stress-induced tubular epithelial damage in the experimental rat hyperoxaluria model. *Medicina (Kaunas)* **57**, 566.
31. Zhu W, Xu YF, Feng Y, Peng B, Che JP, Liu M, Zheng JH (2014) Prophylactic effects of quercetin and hyperoside in a calcium oxalate stone forming rat model. *Urolithiasis* **42**, 519–526.
32. Liebman M, Costa G (2000) Effects of calcium and magnesium on urinary oxalate excretion after oxalate loads. *J Urol* **163**, 1565–1569.
33. Selvam R (2002) Calcium oxalate stone disease: Role of lipid peroxidation and antioxidants. *Urol Res* **30**, 35–47.
34. Song Q, Liao W, He Z, Li D, Dong C, Song C, Yang S (2022) Oxalate induces the ossification of RTECs by activating the JAK2/STAT3 signaling pathway and participates in the formation of kidney stones. *Arch Biochem Biophys* **727**, 109325.
35. Mulay SR, Eberhard JN, Desai J, Marschner JA, Kumar SV, Weidenbusch M, Grigorescu M, Lech M, et al (2017) Hyperoxaluria requires TNF receptors to initiate crystal adhesion and kidney stone disease. *J Am Soc Nephrol* **28**, 761–768.

Appendix A. Supplementary data

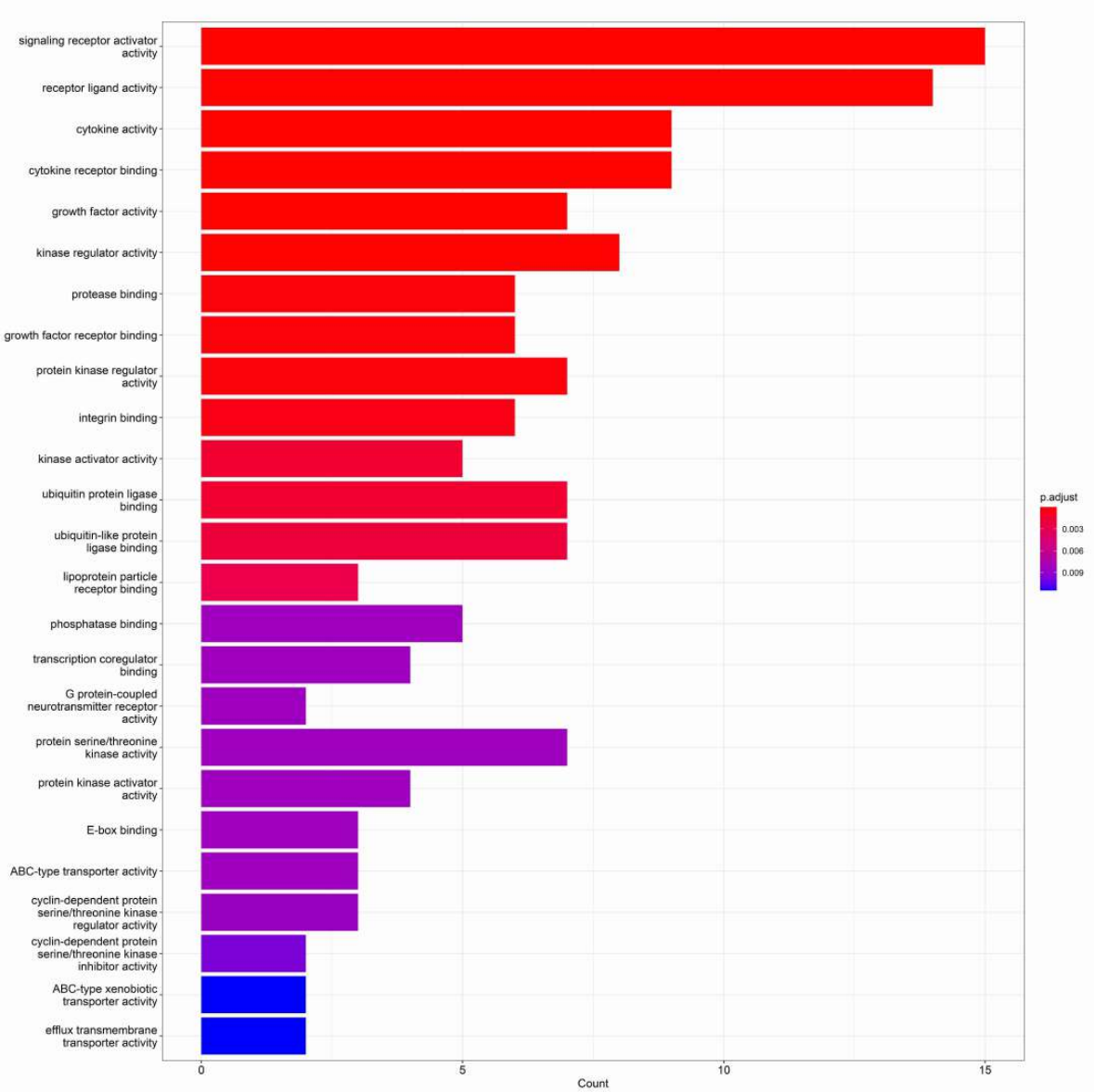

Fig. S1 GO molecular function enrichment bar plot of target genes. The x-axis represents the number of enriched genes (Count), and the y-axis indicates GO molecular function terms. The color denotes the adjusted p-value (p.adjust); darker red corresponds to a smaller adjusted p-value and higher enrichment significance.

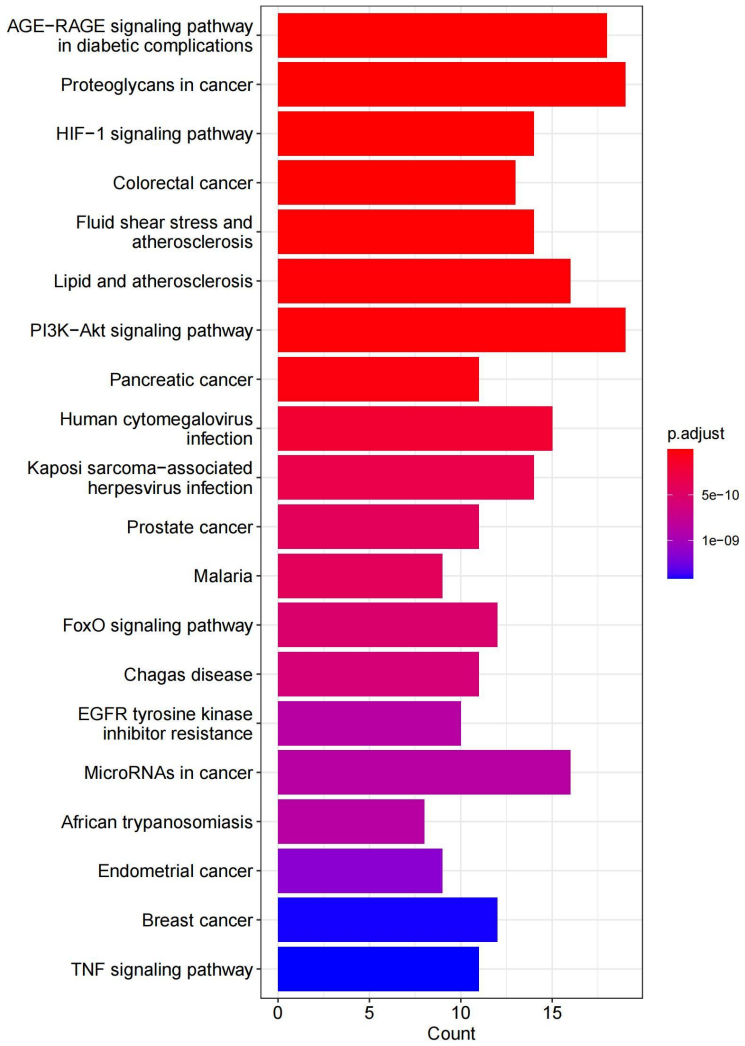

Fig. S2 KEGG pathway enrichment analysis of kidney stone related target genes. The x-axis represents the number of enriched genes (Count), and the y-axis shows the names of enriched KEGG pathways. The color indicates the adjusted *p*-value (*p*.adjust); redder colors correspond to smaller adjusted *p*-value and higher enrichment significance.

Table S5 Compounds detected in four LC-MS/MS conditions with detection count equal to 4.

Name	Count	Proportion
2-(4-Methyl-3-cyclohexen-1-yl)-2-propanyl 6-O-(6-deoxy-α-L-mannopyranosyl)-β-D-glucopyranoside	4	0.6%
4-Indolecarbaldehyde	4	0.6%
Adenine	4	0.6%
Catechin	4	0.6%
Chlorogenic acid	4	0.6%
Guanine	4	0.6%
Guanosine	4	0.6%
L-Histidine	4	0.6%
L-Phenylalanine	4	0.6%
Syringic acid	4	0.6%
Vanillin	4	0.6%
Xanthine	4	0.6%

Table S6 Active medicinal ingredients in the aqueous extract of *O. corniculata* L.

Name	Function	Molecular weight	RT (min)	Area (max.)	Class
(-)-Caryophyllene oxide	Caryophyllene oxide,possesses analgesic and anti-inflammatory activity	220.18212	17.102	3653066.249	terpenoid
(-)-Epigallocatechin	(-)-Epigallocatechin is the most abundant flavonoid in green tea, can bind to unfolded native polypeptides and prevent conversion to amyloid fibrils.	306.07305	6.107	321706212	Flavonoids
(+)-Aphidicolin	Aphidicolin is an inhibitor of DNA polymerase α and δ, prevents mitotic cell division by interfering with the activity of DNA polymerase	320.23189	22.964	51312221.29	Benzene and substituted derivatives
10-Propoxydecanoic acid	O-11 is an analog of the fully saturated, 14-carbon fatty acid myristic acid. O-11 has highly effective and selective effect on Trypanosoma brucei.	242.20288	24.327	47711813.43	Nucleoside and nucleotide analogues
2,5-di-tert-Butylhydroquinone	2,5-Di-tert-butylhydroquinone (DTBHQ), the indirect food additive, regulates the activity of 5-lipoxygenase as well as the activity of COX-2	222.16142	21.443	36748781.33	Furans
2-Amino-1,3,4-octadecanetriol	Has the effect of inhibiting tumor cell proliferation and inducing tumor cell apoptosis	317.29219	20.41	23172309.4	Cinnamic acids and derivatives
2-Furoic acid	2-Furoic acid (Furan-2-carboxylic acid) is an organic compound produced through furfural oxidation	112.01478	1.425	998907110.5	Organooxygen compounds
2-Hydroxycinnamic acid	2-Hydroxycinnamic acid shows inhibitory effects on infection of HIV/SARS-CoV S pseudovirus .	164.04704	12.733	13142724.01	Lactone compounds
4,5-Dicaffeoylquinic acid	4,5-Dicaffeoylquinic acid (Isochlorogenic acid C) possesses potent hepatoprotective and anti-HBV effects.	516.12654	12.72	8981891.908	protease
4-Coumaric acid	p-Hydroxycinnamic acid, a common dietary phenol, could inhibit platelet activity.	164.04704	8.931	56028461.09	Nucleoside and nucleotide analogues
4-Phenylbutyric acid	Benzenebutyric acid is an inhibitor of HDAC and endoplasmic reticulum (ER) stress, used in cancer and infection research.	164.0833	11.991	18716525.21	Lactones
Abacavir	Abacavir is a powerful nucleoside analog reverse transcriptase inhibitor (NRTI) used to treat HIV and AIDS.	264.17194	20.837	34578221.18	Flavonoids
Andrographolide	Andrographolide is a NF-κB inhibitor, which inhibits NF-κB activation through covalent modification of a cysteine residue on p50 in endothelial cells without affecting IκBα degradation or p50/p65 nuclear translocation.	350.20586	17.719	34783525.49	Fatty Acyls
Apigenin	Apigenin is a competitive CYP2C9 inhibitor.	270.05284	17.231	7669828.396	Carboxylic acids and derivatives
Arachidonic acid	Arachidonic acid is an essential fatty acid and a major constituent of biomembranes.	304.2394	23.323	26771629.89	Benzene and substituted derivatives
Betaine	Anti fatty liver, anti-tumor, and blood pressure lowering	117.07903	1.333	352954995.4	Flavonoids
Butylparaben-13C6	Butylparaben is an organic compound, has proven to be a highly successful antimicrobial preservative in cosmetics, also used in medication suspensions, and as a flavoring additive in food.	194.09357	17.64	19883566.7	Organooxygen compounds
Catechin	Catechin inhibits cyclooxygenase-1 (COX-1)	290.07902	8.32	966071035	polyphenolic compounds
Chlorogenic acid	Chlorogenic acid is a major phenolic compound in coffee and tea. It plays several important and therapeutic roles such as antioxidant activity, antibacterial, hepatoprotective, cardioprotective, anti-inflammatory, antipyretic, neuroprotective, anti-obesity, antiviral, anti-microbial, anti-hypertension.	354.09492	9.966	34822806.61	Phenols
cis-Resveratrol	cis-Resveratrol exhibits signifcant antiviral activity.	228.07842	13.47	19566712.61	Flavonoids
Coniferyl aldehyde	trans-Coniferyl aldehyde suppresses 63% of the UV mutable gene expression at 1.20 μM, has the antimutagenicactivities against furylfuramide, Trp-P-1, and activated Trp-P-1.	178.06262	8.099	286901227.2	Benzopyranones
Diosmetin	Diosmetin is a natural flavonoid which inhibits human CYP1A enzyme activity in HepG2 cell.	300.06249	14.234	12880703.19	Coumarins and derivatives
Eicosatetraynoic acid	Eicosatetraynoic acid (ETYA) is a nonspecific inhibitor of cyclooxygenase and lipoxygenase	308.19567	22.205	64984475.38	Cinnamic acids and derivatives
Esculetin	Esculetin is an active ingredient extracted mainly from the bark of Fraxinus rhynchophylla. Esculetin inhibits platelet-derived growth factor (PDGF)-induced airway smooth muscle cells (ASMCs) phenotype switching through inhibition of PI3K/Akt pathway. Esculetin has antioxidant, antiinflammatory, and antitumor activities.	178.02623	10.685	4552874.104	Benzene and substituted derivatives
Esculin	Esculin ameliorates cognitive impairment in experimental diabetic nephropathy (DN), and exerts anti-oxidative stress and anti-inflammatory effects, via the MAPK signaling pathway[2].	340.07933	9.385	5561543.46	Isoflavonoids
Ferulic acid	Ferulic acid is a novel fibroblast growth factor receptor 1 (FGFR1) inhibitor.	194.05714	9.032	71981118.1	Isoflavonoids
Gallic acid	Gallic acid is an antioxidant which can inhibit both COX-2.	170.02075	3.466	42467291.65	Flavonoids
Genistein	Genistein, a soy isoflavone, is a multiple tyrosine kinases inhibitor which acts as a chemotherapeutic agent against different types of cancer, mainly by altering apoptosis, the cell cycle, and angiogenesis and inhibiting metastasis.	270.05287	15.193	4516322.855	Flavonol glycoside compounds
Glycitein	Glycitein is a soybean (yellow cultivar) isoflavonoid; used in combination with other isoflavonoids such as genistein and daidzein to study apoptosis and anti-oxidation processes.	284.06703	12.911	6637211.204	Phenylpropanoic acids
Hispidulin	Hispidulin is a natural flavone with a broad spectrum of biological activities.	300.06328	15.278	20439127.52	Cinnamic acids and derivatives
Hyperoside	Hyperoside, a natural flavonoid, isolated from Camptotheca acuminate, possesses antifungal, anti-inflammatory, anti-viral, anti-oxidative and anti-apoptotic activities.	464.09267	10.983	12259022.62	Benzene and substituted derivatives

Table S6 Continue ...

Name	Function	Molecular weight	RT (min)	Area (max.)	Class
Ibuprofen	Ibuprofen is an anti-inflammatory inhibitor targeting COX-1 and COX-2 .	206.13016	11.672	97806843.05	Flavonoids
Isoferulic acid	trans-isoferulic acid suppresses NO and PGE2 production through the induction of Nrf2-dependent heme oxygenase-1 (HO-1)[2].	194.05753	11.884	39219771.58	Naphthofurans
Isovanillic acid	Isovanillic acid (3-Hydroxy-4-methoxybenzoic acid) is a phenolic acid isolated from isolated from S. frutescens, with Anti-inflammatory activity.	168.04196	6.854	31830685.91	Flavonoids
Kaempferol	Kaempferol inhibits estrogen receptor expression in breast cancer cells and induces apoptosis in glioblastoma cells and lung cancer cells by activation of MEK-MAPK.	286.04692	14.218	27223342.72	Organic compounds
Kahweol	Kahweol is one of the consituents of the coffee from Coffea Arabica with anti-inflammatory anti-angiogenic, and anti-cancerous activities. Kahweol inhibits adipogenesis and increase glucose uptake by AMP-activated protein kinase (AMPK) activation.	314.18501	22.149	13185314.11	Organic compounds
Linolenic acid ethyl ester	Ethyl linolenate is a fatty acid ethyl ester (FAEE). Ethyl linolenate plays an active role in inhibition of the cellular production on melanin with an IC50 of 70 μm.	306.255	25.556	37952215.72	Flavonoids
Luteolin	Luteolin is a falconoid compound, which exhibits anticancer properties.	286.04777	16.118	11306852.12	Phenolic compounds
Mesalamine	5-Aminosalicylic acid acts as a specific PPAR agonist and also inhibits p21-activated kinase 1 (PAK1)	153.04228	2.451	45227707.94	Prenol lipids
Muscone	Muscone is the main active monomer of traditional Chinese medicine musk. Muscone inhibits NF-kappa and NLRP3 inflammasome activation. Muscone remarkably decreases the levels of inflammatory cytokines (IL-1, TNF and IL-6), and ultimately improves cardiac function and survival rate.	238.22908	24.814	41057756.57	Stilbenes
Naringenin	Naringenin is the predominant flavanone in grapefruit; displays strong anti-inflammatory and antioxidant activities.	272.06849	15.535	5071236.041	Phenolic compounds
Neochlorogenic acid	Neochlorogenic acid inhibits phosphorylated NF-kappa p65 and p38 MAPK activation.	354.09495	9.162	677041979.2	Flavonoids
Oleanolic acid	Oleanolic acid (Caryophyllin) is a natural compound from plants with anti-tumor activities.	438.34866	25.766	62232114.06	flavonoids
Piceatannol	Piceatannol is a selective inhibitor of protein tyrosine kinase Syk.	244.07341	4.376	3360733.58	Flavonoids
Pyrogallol	Pyrogallol is a polyphenol compound, which has anti-fungal and anti-psoriatic properties.	126.03053	3.398	14801894.27	Phenolic compounds
Quercetin	Quercetin is a natural flavonoid which activates or inhibits the activities of a number of proteins.	302.04252	14.831	11795004.76	Flavonoids
Quercetin-3β-D-glucoside	Quercetin-3-glucoside is a naturally occurring polyphenol that has antioxidant, anti-proliferative, and anti-inflammatory properties.Quercetin-3-glucoside alleviates ethanol-induced hepatotoxicity, oxidative stress, and inflammatory responses via the Nrf2/ARE antioxidant signaling pathway[1].	464.09538	11.208	23203617.71	alkaloid
Schaftoside	Schaftoside is a flavonoid found in a variety of Chinese herbal medicines, such as Eleusine indica. Schaftoside inhibits the expression of TLR4 and Myd88.	564.14616	11.766	6234554862	Prenol lipids
Sinapinic acid	Sinapinic acid shows antioxidant and antidiabetic activities.	224.06799	9.728	5192952.627	Flavonoids
Taxifolin	Taxifolin exhibits important anti-tyrosinase activity.	304.05763	7.025	9901202.873	Myristic acid ester
Trigonelline	Trigonelline, an alkaloid with potential antidiabetic activity, is present in considerable amounts in coffee.	137.04733	1.418	2902796404	sphingoid
Ursolic acid	Ursolic acid(Bungeolic acid) is a natural pentacyclic triterpenoid carboxylic acid, exerts anti-tumor effects and is an effective compound for cancer prevention and therapy.	456.36012	24.657	2927431.512	Organic compounds
Vitexin	Vitexin has a wide range of pharmacological effects, including anti-oxidant, anti-cancer, anti-inflammatory, anti-hyperalgesic, and neuroprotective effects.	432.1043	12.289	100679232.1	Click chemistry reagent